Journal of Biomedical Optics 6(4), 474–479 (October 2001)

In vivo burn depth determination by high-speed fiber-based polarization sensitive optical coherence tomography

B. Hyle Park
Beckman Laser Institute and Medical Clinic
University of California
1002 Health Sciences Road East
Irvine, California 92612
and
Wellman Laboratories of Photomedicine
Massachusetts General Hospital
50 Blossom Street BAR 724
Boston, Massachusetts 02114

Chris Saxer
Shyam M. Srinivas
J. Stuart Nelson
Beckman Laser Institute and Medical Clinic
University of California
1002 Health Sciences Road East
Irvine, California 92612

Johannes F. de Boer
Beckman Laser Institute and Medical Clinic
University of California
1002 Health Sciences Road East
Irvine, California 92612
and
Wellman Laboratories of Photomedicine
Massachusetts General Hospital
50 Blossom Street BAR 724
Boston, Massachusetts 02114

Abstract. We report the first application of high-speed fiber-based polarization sensitive optical coherence tomography (PS-OCT) to image burned tissue *in vivo*. Thermal injury denatures collagen in skin and PS-OCT can measure the reduction in collagen birefringence using depth resolved changes in the polarization state of light propagated in, and reflected from, the tissue. Stokes vectors were calculated for each point in a scan and birefringence relative to incident polarization determined using four incident polarization states. Using a high-speed fiber-based PS-OCT system on rat skin burned for varying periods of time, a correlation between birefringence and actual burn depth determined by histological analysis was established. In conclusion, PS-OCT has potential use for noninvasive assessment of burn depth.
 [DOI: 10.1117/1.1413208]

Keywords: burn depth; polarization; fiber optics; coherent optical systems.

Paper JBO-001012 received Feb. 15, 2001; revised manuscript received May 31, 2001; accepted for publication June 28, 2001.

1 Introduction

Burns are a leading cause of accident-related death in the United States, exceeded in numbers only by automobile crashes and falls.[1,2] Approximately 2 million people suffer serious burns each year; of these 115 000 are hospitalized and 12 000 die.[1,2] These injuries can be categorized by causation and burn severity. Burns can be defined as injury to the skin and deeper tissues caused by hot liquids, flames, radiant heat, direct contact with hot solids, caustic chemicals, electricity, or electromagnetic (nuclear) radiation. Burn severity is related to depth, extent, and age of the victim. Burns are classified by depth into first, second, and third degree injuries. First degree burns cause redness and pain (e.g., sunburn). Second degree burns are marked by blisters (e.g., scald by hot liquid). In third degree burns, both the epidermis and dermis are destroyed, and underlying tissue may also be damaged. Thermal injury of human skin allows for infection, which is the most common cause of morbidity and mortality in victims. Making the distinction between second- and third-degree burns is difficult; the burn surgeon will often observe the injury over the course of several days before making an educated guess regarding burn depth.[3] Clearly, a noninvasive method of assessing burn depth would be beneficial to the patient and surgeon alike. Recently developed techniques include the use of indocyanine green dye fluorescence, vital dyes, fluorescein fluorometry, laser Doppler flowmetry (LDF), thermography, ultrasound, nuclear magnetic resonance imaging, and visible reflectance spectroscopy.[4–7] Much research in this general area has been focused on LDF. Burns damage dermal arterioles, capillaries, and venules, resulting in reduced blood flow which can be detected by LDF. However, due to the long coherence length optical sources required, LDF cannot provide a depth resolved image of blood flow, but instead measures perfusion over an entire volume of tissue. Problems with methodology and accuracy have limited the use of LDF, and many of the other techniques mentioned above, leaving clinical observation as the standard for diagnosis.

Polarization-sensitive optical coherence tomography (PS-OCT) is a recently developed imaging technique that can potentially assess burn depth *in vivo*. Optical coherence tomography (OCT) allows high-resolution cross-sectional imaging of tissue microstructure,[8] analogous to ultrasound imaging except that infrared light rather than acoustic waves are used. An optical beam is focused into the tissue, and the echo time delay of light reflected from internal microstructure at different depths is measured by interferometry. Image information is obtained by performing repeated axial (depth) measurements at different transverse positions by scanning the optical beam across the tissue. The resulting data constitute a two-

Address all correspondence to B. Hyle Park, Tel: 617-724-5532; Fax: 617-726-4103; Email: hylepark@helix.mgh.harvard.edu

1083-3668/2001/$15.00 © 2001 SPIE

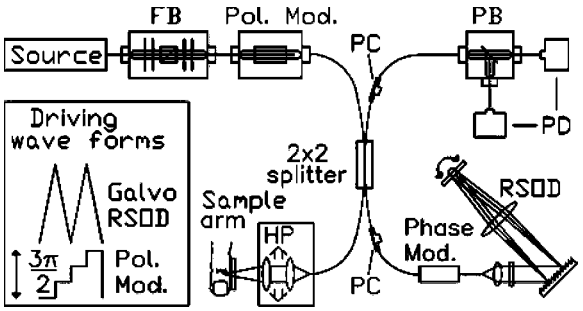

Fig. 1 Fiber-based PS-OCT system. FB: fiber bench with polarizer, Pol. Mod.: polarization modulator, PC: static polarization controller, PB: polarizing beam splitter, RSOD: rapid scanning optical delay line, PD: photodiodes, and HP: handpiece on motorized linear translation stage (velocity 1.87 mm/s).

dimensional map of the backscattering or reflectance from internal architectural morphology and cellular structures in the tissue. PS-OCT takes advantage of any polarization changing properties of the tissue under study.[9,10] Polarized light is emitted from the source arm of the system and the change in the polarization state of the light returned from the sample arm is measured. This technique takes advantage of the fact that skin contains collagen, a birefringent material. At temperatures between 56 and 65°C, collagen denatures, and loses its birefringence.[11] Normal and burned skin differ in their natural collagen content which is manifested by a difference in their ability to alter the polarization state of light that has passed through and been reflected back from them. By analyzing the polarization state of light reflected from various depths in a sample, PS-OCT is able to provide information on the content and condition of collagen and, therefore, the depth of thermal injury. We have developed a high-speed fiber-based system and found a correlation between burn depth, determined by histological analysis, and degree of phase retardation by depth, determined from our PS-OCT scans.

2 Materials and Methods

Trials were performed *in vivo* on seven Sprague–Dawley rats (~300 g) in full compliance with an experimental protocol approved by the Institutional Animal Care and Use Committee at the University of California, Irvine. After anaesthetizing animals with an intraperitoneal injection of ketamine (87 mg/kg) and xylazine (13 mg/kg), their backs were shaved and treated with Nair® lotion hair remover (Carter-Wallace, NY). Burns of 5, 20, and 30 s durations were initiated on contralateral sites of the exposed skin on each rat using a brass rod heated to 75°C in a water bath. *In vivo* PS-OCT scans were taken of the four sites (one of each burn duration and normal skin control) while the animals remained anesthetized.

A schematic of the PS-OCT system used is illustrated in Figure 1. Here we will give a brief description of the system, described in greater detail by Saxer et al.[12] Previous PS-OCT systems[13] were based on free space interferometers composed of bulk optical components that allow for precise control of the polarization state of light in the reference arm and incident in the sample arm. However, system alignment and positioning of the sample arm relative to a biological sample can be very difficult. A fiber-based PS-OCT system eases both alignment and orientation of the sample arm but inherent birefringence in an optical fiber can alter the polarization state of light transmitted through it. Rather than using polarization-maintaining fibers and losing phase information, fiber birefringence is compensated by data analysis described in a later section. Light from a low coherence source (centered at 1310 nm with a 75 nm bandwidth) is passed through optical components to select the polarization state of the source with the highest power. This light is sent to an electro-optical polarization modulator controlled with a four step driving function designed to alter the polarization state, denoted by vectors 1, 2, 3, and 4, in $\pi/2$ increments spanning a grand circle on Poincaré's sphere [Figure 2(a)]. A 2×2 fiber splitter sends the light to the reference and sample arms. The reference arm, the primary component of which is a rapid scanning optical delay line (RSOD),[14,15] provides depth resolution. Incident power on the sample is approximately 2.5 mW. Lateral resolution is controlled by a motorized stage in the sample arm, and light reflected back from the sample arm is combined with that from the reference arm, where phase and amplitude of the interference pattern in two orthogonal detectors for all four incident polarizations are recorded. A single scan (3.47 mm $\times$ 2 mm with 10 μm$\times$10 μm resolution) takes 2 s to acquire.

In an open air PS-OCT system, calculating the amount of birefringence in a sample is fairly straightforward. The incident polarization state does not vary and can be controlled so that it is circular. This insures insensitivity to the direction of the optic axis of the sample, which, for birefringent materials, must be constrained to the QU-plane in a Poincaré sphere representation. In this case, the change in the polarization state can be completely determined from the difference between the known incident polarization state and that reflected or backscattered from a particular point in the scan.[13,16] However, since fibers introduce a constant but unknown birefringence, determination of the same information in a fiber-based system is more complex. The two main complications are that the incident polarization state is no longer known and that the overall direction of the optic axis (from the combination of sample and fibers) is no longer constrained to the QU-plane.

Both these problems are solved by probing the sample with four polarization states and with the knowledge that the fibers preserve orthogonality between these states. The incident polarization state is now taken as the polarization state of light returning from the surface of the sample. Since, in the Poincaré sphere representation, polarization states 1 and 3 are π radians apart and differ only by a negative sign in their Stokes' vector representations, these two traces can be averaged to reduce noise, resulting in incident polarization state $\mathbf{I}_1$. The same can be done with traces 2 and 4, resulting in $\mathbf{I}_2$ [Figure 2(b)]. $\mathbf{I}_1$ and $\mathbf{I}_2$ are compared to Stokes vectors returning from deeper in the sample, denoted by states $\mathbf{I}_1'$ and $\mathbf{I}_2'$. The calculation involves first determining an optic axis and then a degree of phase retardation about that axis. A single rotation, for example, from $\mathbf{I}_1$ to $\mathbf{I}_1'$, determines a plane of possible optic axes spanned by the sum and cross product of the two states. The intersection of the two planes, one determined by $\mathbf{I}_1$ and $\mathbf{I}_1'$ [Figure 2(c)], the other determined from $\mathbf{I}_2$ and $\mathbf{I}_2'$ [Figure 2(d)], is taken as the overall optic axis, $\mathbf{A}$ [Figure 2(e)]. The final step in the analysis is determining the degree of phase retardation over this optic axis. θ_1 may be

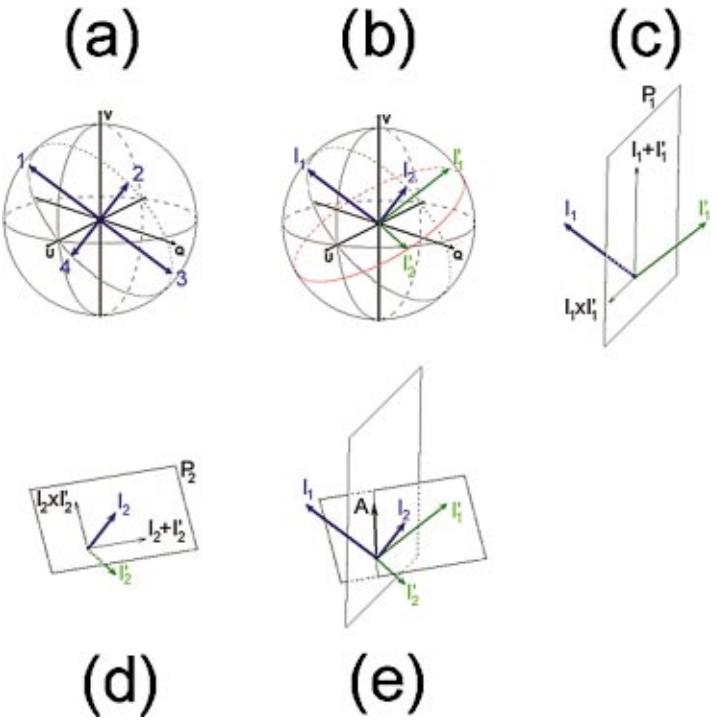

Fig. 2 (a): Four orthogonal polarizations of light at the fiber tip used to probe the sample exist within a grand circle in Poincaré's sphere. (b)–(e) These figures illustrate an example of a birefringence calculation. (b); The polarization states at the surface, I_1 and I_2, are depicted on Poincaré's sphere along with the polarization states reflected from a particular point in the sample, I_1' and I_2'. (c) Plane P_1 is determined from I_1 and I_1'. (d) Plane P_2 is determined from I_2 and I_2'. (e) The intersections of planes P_1 and P_2 are taken as the combined optic axis A.

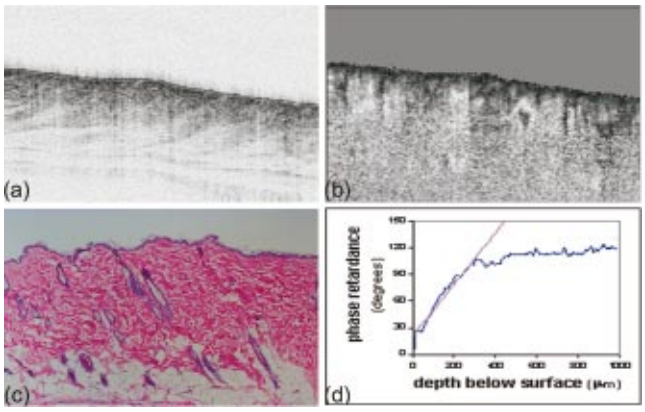

Fig. 3 Normal rat skin. (a) OCT image, (b) phase map, (c) histology, and (d) plot of phase retardance vs depth.

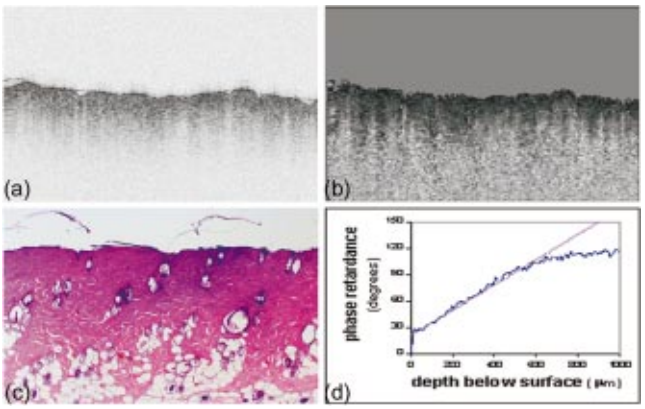

Fig. 4 Rat skin burned for 30 s at 75°C. (a) OCT image, (b) phase map, (c) histology, and (d) plot of phase retardance vs depth. The dimensions of the histological images and phase maps are 3.2 mm by 2 mm, and depths in the graphs are measured from the tissue surface. The absence of speckle above the sample surface is due to the fact that calculation of the phase map was only performed below the surface.

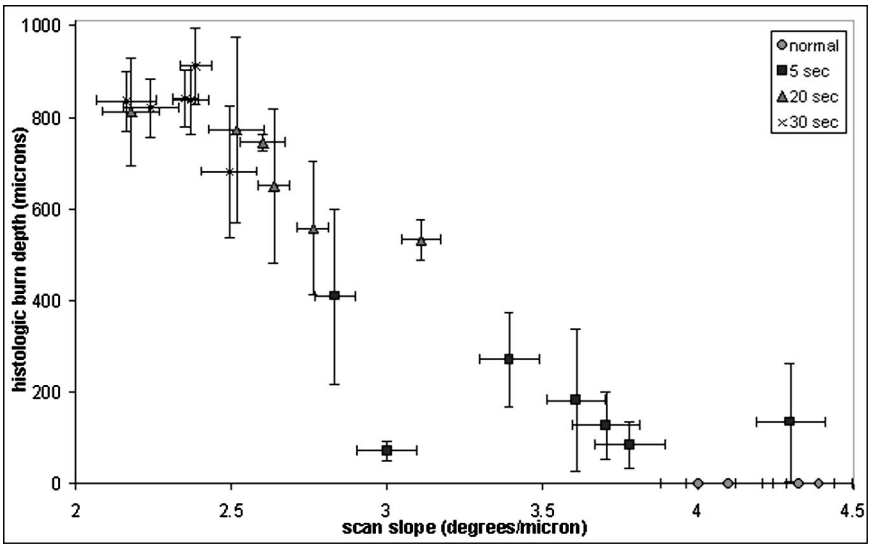

Fig. 5 Overall graph of burn depth determined by histological analysis as a function of phase retardation from PS-OCT, by burn duration. The A lines in an image are averaged to generate a graph of degree of phase retardation vs depth into the tissue. The slopes of the roughly linear portions of these graphs are determined by least-squares fitting, and the slope and error reported as a measure of phase retardation (scan slope).

defined as the degree of rotation about $\mathbf{A}$ that takes $\mathbf{I}_1$ to $\mathbf{I}_1'$, and θ_2 is defined analogously. The expectation is that the two rotation angles are equal, however, in practice they differ slightly due to noise. The overall phase retardation is taken as the intensity weighted average of the angles,

$$\theta = \frac{|\mathbf{I}_1'|\,\theta_1 + |\mathbf{I}_2'|\,\theta_2}{|\mathbf{I}_1'| + |\mathbf{I}_2'|}.$$

These values are encoded on a gray scale with black and white representing rotation of 0 and π radians, respectively. The A lines are then averaged to generate a graph of degree of phase retardation versus depth into the tissue. The slope of the roughly linear portion of the graph is least-squares fitted and the slope and error reported as measures of tissue birefringence.

After scans were taken from normal and burned skin sites, tissues were excised with 4 mm punch biopsies (Miltex, Lake Success, NY) and processed with a regressive hematoxylin and eosin (H&E) stain. Histological analysis was used to determine burn depth as assessed by the following three main criteria.[17] The first criterion was examination of the state of viable adnexal structures, such as hair follicles and sweat glands. If such structures appeared damaged, it was inferred that thermal injury reached at least to that depth. The second criterion was the color of the histological section as regressive H&E stain goes from pink in normal skin to a purple color in the presence of denatured dermal collagen. The final criterion used was the presence of hyalinization. Normal dermis is composed of collagen fibers and fibroblasts oriented roughly parallel to the skin surface. When skin is thermally damaged, fibers lose their linearity and fuse with their neighbors to create a glass-like appearance from the dense coagulation of collagen. Signs of such hyalinization were taken to indicate that thermal injury had occurred to that depth. Each biopsy typically yielded two slides with between six and ten sections each and were examined under an Olympus BH-2 (Olympus, Melville, NY) microscope with a reticule eyepiece. Using the ruler built into the microscope, burn depth in micrometers (± 5 μm) was measured for each histological section according to the previously mentioned criteria. Average burn depth for a particular biopsy and its standard deviation were determined from individual measurements of all sections obtained from that particular biopsy.

3 Results

Figures 3 and 4 show examples of normal, unburned rat skin and skin burned for 30 s at 75°C, respectively. Figures 3(c) and 4(c) are histological sections and comparison between the two highlights some of the previously mentioned criteria used for burn depth determination. The most notable difference in the general appearance of the tissue is the absence or presence of hyalinization. Normal skin in Figure 3(c) has a fairly uniform density of collagen fibers throughout the dermis that is not visible in the upper regions of Figure 4(c), due to collagen coagulation. The effects of thermal injury are also readily apparent in the PS-OCT scans [Figures 3(b) and 4(b)]. In the burned tissue, the darker region extends to a visibly greater depth than in normal skin, indicating a lesser degree of birefringence in that tissue. This difference is quantified in the phase retardance plots [Figures 3(d) and 4(d)]. The slopes and standard deviations determined by least-squares fits of the linear portions of these graphs are calculated. Plotting scan slope versus histologic burn depth yielded the correlation shown in Figure 5.

4 Discussion

The primary source of birefringence in skin is collagen, a weakly birefringent material with a fairly uniform distribution

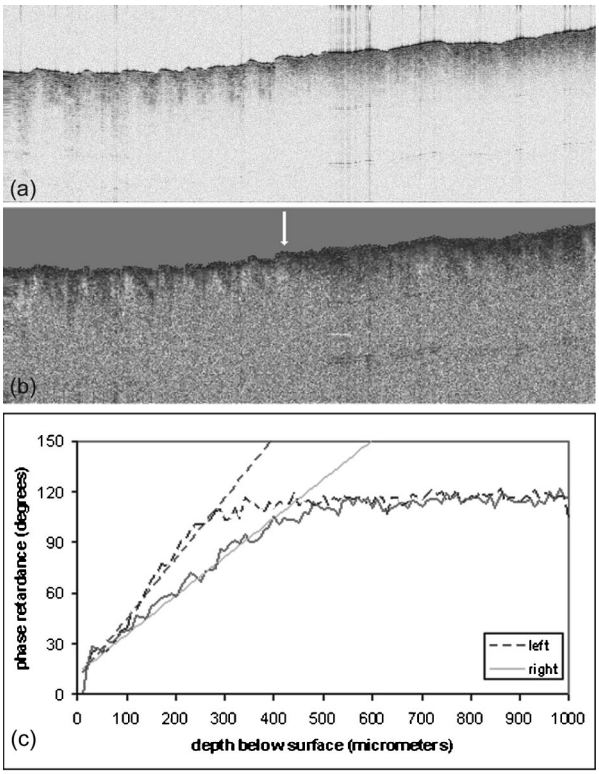

Fig. 6 (a) and (b) OCT image and PS-OCT image across the boundary, marked by the white arrow, of a burned region (normal skin to the left of the arrow; burned tissue on the right). Image corresponds to a 6 mm by 2 mm cross sectional area. The absence of speckle above the sample surface is due to the fact that the phase map was only calculated for points below the surface. (c) Graph depicting phase retardance as a function of depth for the unburned and burned areas of the image.

in skin. The degree of phase retardation depends on two factors: distance through the tissue that the light has traveled, and density of natural collagen. The variation with distance is evident in the first 300–500 μm in depth in the PS-OCT scans; as the depth increases, the degree of phase retardation increases [Figures 3(c) and 4(c)]. After this initial 300–500 μm, the graph asymptotically approaches approximately 115°. This may be attributed to depolarization due to scattering, which reduces the signal intensity as well as randomizing the polarization state of the light. The amount of scattering in tissue is also a function of path length, and these effects become more pronounced at deeper depths in the PS-OCT scans, effectively randomizing the Stokes vectors. Monte Carlo calculation of randomized polarization states returning from the tissue yields an average degree of phase retardation of $114.9° \pm 0.1°$, confirming the asymptotic behavior seen in the graphs.

Figure 5 indicates the effects of the ratio of normal versus denatured collagen on the change in phase retardation. At temperatures between 56 and 65 °C, collagen denatures and loses its birefringence. The application of 75 °C burns for 5, 20, and 30 s results in areas of skin with lowered fractions of natural collagen. Comparing areas burned for 5 and 30 s, respectively, light that has traveled a certain depth in the less burned skin will be retarded more than light traveling through the same depth in the tissue with more collagen denaturation. This is seen in Figure 5, where the degree of phase retardation per unit depth decreases with increasing burn depth.

The boundaries of a burn can also be determined using PS-OCT. Figure 6(a) (6×2 mm, 10×10 μm/pixel) shows a scan taken across the boundary of a 30 s burn. Figure 6(b) reveals the difference in phase retardation as a function of depth for the left and right portions of the image. The normal, unburned part in the left part of the scan corresponds to the graph with the higher slope, as expected. The most important feature between normal skin on the left side of the image and burned tissue on the right is the readily visible boundary of the burned area clearly demarcated by the white arrow in the PS-OCT scan.

These preliminary results demonstrate the potential ability of PS-OCT to assess burn depth *in vivo*. A good correlation between degree of phase retardation as a function of depth and burn depth as determined by histology for rat skin has been demonstrated for the burn model used. In extending these results to humans, a relative consideration is imaging depth; a burn in humans, where the skin is thicker than that in rats, can extend much deeper than the 1.0–1.5 mm penetration depth of the scans. However, a more severe burn will denature more surface collagen than a less severe burn and so a measurement of the reduction in collagen in the first millimeter of skin will still reveal information on overall burn depth. Another consideration is the effect of various types of burns, ranging from flash burns to longer but lower temperature burns. The correlation between the degree of collagen denaturation detectable by PS-OCT and the burn depth in these cases requires further study. As scanning speed and imaging depth increases, so should accuracy, and so as PS-OCT evolves, it could become useful for noninvasive assessment of burn depth *in vivo*.

Acknowledgments

Research grants from the Whitaker Foundation (26083, JFdB), Office of Naval Research (N00014-94-1-0874), National Institute of Health (GM58785), U.S. Department of Energy and the Beckman Laser Institute Endowments are gratefully acknowledged.

References

1. Heat burn injuries, Bulletin/U.S. Department of Labor, Bureau of Labor Statistics (1990).
2. J. M. Stein, ''Burn,'' Microsoft® Encarta® Online Encyclopedia 2000 http://encarta.msn.com © 1997–2000 Microsoft Corporation, Redmond, WA (2000).
3. P. A. Brigham and E. McLoughlin, ''Burn incidence and medical care use in the United States: Estimates, trends, and data sources,'' *J. Burn Care Rehabil.* **17**, 95–107 (1997).
4. R. L. Sheridan et al., ''Burn depth estimation by use of indocyanine green fluorescence: Initial human trial,'' *J. Burn Care Rehabil.* **16**, 602–604 (1995).
5. D. Heimbach, L. Engrav, B. Grube, and J. Marvin, ''Burn depth: A review,'' *World J. Surg.* **16**, 10–15 (1992).
6. D. H. Park, J. W. Hwang, K. S. Jang, D. G. Han, K. Y. Ahn, and B. S. Baik, ''Use of laser Doppler flowmetry for estimation of the depth of burns,'' *Plast. Reconstr. Surg.* **101**, 1516–1523 (1998).
7. E. K. Yeong, R. Mann, M. Goldberg, L. Engrav, and D. Heimbach, ''Improved accuracy of burn wound assessment using laser Doppler,'' *J. Trauma* **40**, 956–962 (1996).

8. G. J. Tearney, M. E. Brezinsky, B. E. Bouma, S. A. Boppart, C. Pitris, J. F. Southern, and J. G. Fujimoto, ''In vivo endoscopic optical biopsy with optical coherence tomography,'' *Science* **276**, 2037–2039 (1997).
9. J. F. de Boer, T. E. Milner, M. J. C. van Gemert, and J. S. Nelson, ''Two-dimensional birefringence imaging in biological tissue by polarization-sensitive optical coherence tomography,'' *Opt. Lett.* **22**, 934–936 (1997).
10. M. J. Everett, K. Schoenenberger, B. W. Colston, and L. B. da Silva, ''Birefringence characterization of biological tissue by use of optical coherence tomography,'' *Opt. Lett.* **23**, 228–230 (1998).
11. J. F. de Boer, S. M. Srinivas, A. Malekafzali, Z. Chen, and J. S. Nelson, ''Imaging thermally damaged tissue by polarization sensitive optical coherence tomography,'' *Opt. Express* **3**, 212–218 (1998).
12. C. E. Saxer, J. F. de Boer, B. H. Park, Y. Zhao, Z. Chen, and J. S. Nelson, ''High-speed fiber-based polarization-sensitive optical coherence tomography of *in vivo* human skin,'' *Opt. Lett.* **25**, 1355–1357 (2000).
13. J. F. de Boer, T. E. Milner, and J. S. Nelson, ''Determination of the depth-resolved Stokes parameters of light backscattered from turbid media by use of polarization-sensitive optical coherence tomography,'' *Opt. Lett.* **24**, 300–302 (1999).
14. G. J. Tearney, B. E. Bouma, and J. G. Fujimoto, ''High speed phase and group delay scanning with a grating based phase control delay line,'' *Opt. Lett.* **22**, 1811–1813 (1997).
15. A. M. Rollins, M. D. Kulkarni, and S. Yazdanfar, ''*In vivo* video rate optical coherence tomography,'' *Opt. Lett.* **3**, 219–229 (1998).
16. C. F. Bohren and D. R. Huffman, *Absorption and Scattering of Light by Small Particles*, John Wiley, New York (1998).
17. T. W. Panke and C. G. McLeod, *Pathology of Thermal Injury: A Practical Approach*, Grune & Stratton, Orlando, FL (1985).